Zero-Dimensional Gua$_3$SbCl$_6$ Crystals as Intrinsically Reabsorption-Free Scintillators for Radiation Detection

Matteo L. Zaffalon, Ye Wu, Francesca Cova, Luca Gironi, Xiaoming Li,* Valerio Pinchetti, Yang Liu, Muhammad Imran, Alessia Cemmi, Ilaria Di Sarcina, Liberato Manna,* Haibo Zeng,* and Sergio Brovelli*

The search for efficient, re-absorption-free scintillators has recently focused the attention on antimony-based halides, which exhibit largely Stokes shifted luminescence due to radiative recombination of excitons self-trapped (STE) in strongly Jahn–Teller distorted Sb^{3+} color centers. Here, the synthesis of a hybrid structure is reported with chemical formula (C$_{13}$H$_{14}$N$_3$)$_3$SbCl$_6$ consisting of spatially isolated [SbCl$_6$]$^{3-}$ octahedra separated by organic N,N'-diphenylguanidinium (Gua) molecules. The optical properties of this material are mainly determined by the inorganic component and are characterized by a pronounced Stokes shift of ≈1.3 eV and a room-temperature photoluminescence (PL) efficiency of up to 85%. Remarkably, highly efficient radioluminescence (RL) is observed with scintillation light yields of ≈2000 ph MeV^{-1} using both soft X-rays and a 124 keV gamma source. Temperature-dependent PL and RL measurements confirm the minor role of non-radiative channels, which are completely suppressed below 100 K. Thermally stimulated luminescence measurements suggest that the traps in Gua$_3$SbCl$_6$ crystals have a significantly large energy depth distribution below the absorbing state.

1. Introduction

The detection of high-energy photons and ionizing particles is of outmost importance for a wide range of scientific and technological areas including high-energy physics,[1] astronomy,[2] geology,[3] industrial, and environmental monitoring,[4] homeland security,[5] oil extraction[6] as well as in medical diagnostic[7]

and space exploration.[8] As of today, radiation detection is mostly performed using scintillating materials that convert ionizing radiation into ultraviolet or visible light that is then collected and turned into an electrical signal by efficient photo-detectors (e.g., photodiodes or photomultipliers) coupled to the scintillator body.[9] In general, scintillating materials must have a high atomic number (Z) to ensure high radiation cross-section ($\propto Z^n$, with $n = 1$–5 depending on the type of interaction),[10] high radiation hardness for long-term operation, good yield proportionality, and they must not contain radioactive isotopes to minimize background noise in rare event experiments. Several photophysical parameters further determine the scintillator performance, above all, the energy resolution, the decay time[11] and the light yield (LY, i.e., the number of emitted photons per 1 MeV of absorbed energy).[12] The LY is pivotal for energy resolution (the theoretical limit of the relative full width at half maximum resolution is proportional to $(\sqrt{LY})^{-1}$)[13] and depends on the efficiency of radiation-to-light conversion and of light outcoupling toward photodetectors coupled to the scintillator.[13a,14] Therefore, decoupling of the emission and absorption spectra is required to eliminate otherwise dramatic reabsorption losses.[15] Currently, the largest share of the market is occupied by inorganic

M. L. Zaffalon, F. Cova, V. Pinchetti, S. Brovelli
Dipartimento di Scienza dei Materiali
Università degli Studi Milano Bicocca
Via R. Cozzi 55, IT-20125 Milano, Italy
E-mail: sergio.brovelli@unimib.it

Y. Wu, X. Li, Y. Liu, H. Zeng
MIIT Key Laboratory of Advanced Display Materials and Devices
Institute of Optoelectronics & Nanomaterials
School of Materials Science and Engineering Nanjing University of Science and Technology
Nanjing 210094, China
E-mail: lixiaoming@njust.edu.cn; zeng.haibo@njust.edu.cn

Y. Wu, L. Manna
Istituto Italiano di Tecnologia
Via Morego 30, IT-16163 Genova, Italy
E-mail: liberato.manna@iit.it

L. Gironi
Dipartimento di Fisica
Università degli Studi Milano Bicocca
Piazza della Scienza 3, IT-20126 Milano, Italy

**ADVANCED
SCIENCE NEWS**

www.advancedsciencenews.com

**ADVANCED
FUNCTIONAL
MATERIALS**

www.afm-journal.de

scintillator crystals[16] that provide high LY and spectroscopic capabilities but suffer from high cost, fragility, hygroscopicity, heavy-weight, and cannot be produced in large sizes or volumes.[17]

In this framework, metal halides and in particular lead halide perovskites are attracting growing attention as alternative affordable scintillating materials because of their scalable low temperature (up to a few hundred degrees Celsius) synthesis, high average Z, defect tolerance and tuneable, near unity efficient excitonic luminescence.[18] More recently, in the attempt to reduce possible harmful effects of toxic lead, lead-free low dimensional halides have been introduced as effective scintillators,[18a,19] also prized for their characteristic intragap luminescence originating from the radiative recombination of excitons localized in isolated structural units or dopant sites.[20] Among these systems, antimony halides combine a relatively high average atomic number (Z_{Sb} = 51) and highly efficient and intrinsically Stokes-shifted visible luminescence[21] that ensures reabsorption free emission without the need for further doping.[20a,21,22] In such systems, unperturbed $[SbX_6]^{3-}$ octahedra (where X is a halogen atom) give rise to sharp absorption peaks in the near UV region ($\approx$3–3.5 eV) due to photoexcitation of the Sb^{3+} centers from their ground state to their $^3P_1$ state.[23] Because of the non-spherical symmetry of the P-states, upon excitation the $[SbX_6]^{3-}$ octahedra undergo strong asymmetrical Jahn-Teller distortion[24] that leads to the formation of the characteristic self-trapped exciton (STE) states $\approx$1 eV below the band-edge energy.[22a,e,h,i,25] On the other hand, the spin-forbidden nature of the STE dipole transition in antimony centers is reflected in an inherently slow decay rate, in stark contrast to the Pb-based counterparts that exhibit sub-nanosecond luminescence dynamics.[26] Despite this potential, as of today, the very few examples of Sb halide-based scintillators have been focused only on X-ray detection and no study has tackled the scintillation process in detail. In addition, antimony chloride systems combined with organic moieties in a hybrid organic–inorganic scintillator could be interesting materials for fast neutron detection that is traditionally performed using hydrogen-rich organic scintillators and exploits a detection mechanism based on the elastic scattering of neutrons on similar-mass hydrogen atoms.[27] However, not much is known about the suitability of these systems for gamma detection as well as on the details of trapping and detrapping mechanisms involved in the scintillation process.

Figure 1. a) Experimental and simulated PXRD patterns of Gua_3SbCl_6 powders at 298 K. b,c) Structures of an individual Gua^+ cation and a six-coordinated $[SbCl_6]^{3-}$ octahedron. d) Configuration of a $2 \times 3 \times 2$ supercell of Gua_3SbCl_6 (H atoms have been hidden for clarity).

Here we aim to contribute to this field by investigating the scintillation properties of a hybrid organic–inorganic zero-dimensional antimony chloride system, namely Gua_3SbCl_6, which consists of alternating layers of $[SbCl_6]^{3-}$ octahedra separated by N,N'-diphenylguanidinium (Gua^+, $C_{13}H_{14}N_3^+$) cations. Concomitant optical and radiometric experiments show that the optical properties of Gua_3SbCl_6 are determined by the absorption by isolated $[SbCl_6]^{3-}$ units and that both the photoluminescence (PL) and the radioluminescence (RL) are due to the essentially purely radiative decay of the Sb-STEs. This leads to light yields of up to 2000 ph MeV^{-1} using ^{57}Co as a 120 keV gamma source, despite the relatively low density of the material (1.468 g cm^{-3}). Finally, thermally stimulated luminescence (TSL) experiments, performed here for the first time on Sb halides, reveal the signature of thermally activated de-trapping from defect sites.

L. Gironi
INFN Sezione Milano – Bicocca
Piazza della Scienza 3, Milano IT-20126, Italy

Y. Liu
CINBIO
Universidade de Vigo
Materials Chemistry and Physics Group
Department of Physical Chemistry
Campus Universitario Lagoas Marcosende
Vigo 36310, Spain

M. Imran
Department of Electrical and Computer Engineering
University of Toronto
10 King's College Road, Toronto, Ontario M5S 3G4, Canada

A. Cemmi, I. Di Sarcina
ENEA Fusion and Technology for Nuclear Safety and Security Department
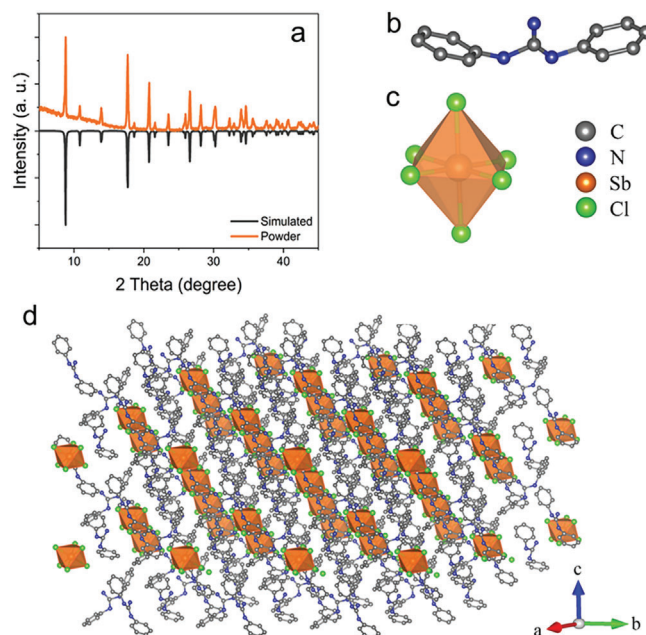Casaccia R.C., Rome 00123, Italy

2. Results and Discussion

Gua_3SbCl_6 powders were prepared by mixing N,N'-diphenylguanidine monohydrobromide (Gua-HBr) and $SbAc_3$ powders in hydrochloric acid solution directly. The detailed synthesis steps of $(Gua)_3SbCl_6$ powders, single crystals (SCs) and material characteristics can be found in the Experimental Section. The crystal structure of the obtained $(Gua)_3SbCl_6$ SCs was determined by single-crystal X-ray diffraction (SCXRD) at 298 K. The powder X-ray diffraction (PXRD) pattern of the as-synthesized powders in **Figure 1**a is consistent with the simulated structure of Gua_3SbCl_6 SCs. As illustrated in Figure 1b–d and Figure S1 (Supporting Information), six-coordinated $[SbCl_6]^{3-}$ octahedra are isolated by bulky Gua^+ cations, adopting a trigonal R3 symmetry. The details of lattice
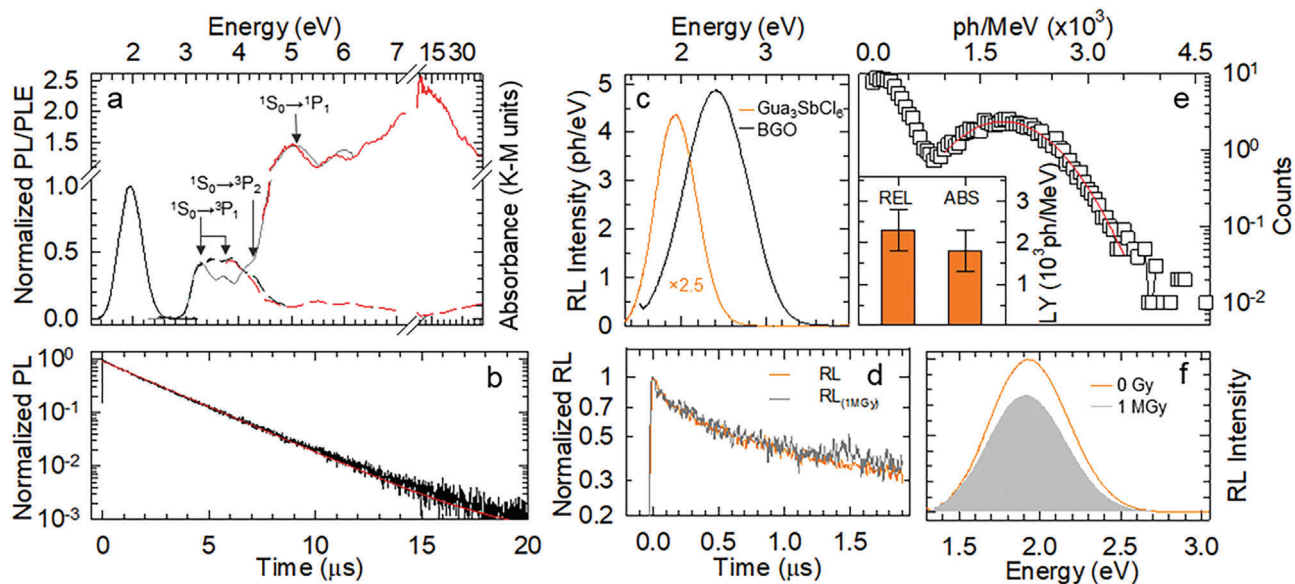
**ADVANCED
SCIENCE NEWS**

www.advancedsciencenews.com

**ADVANCED
FUNCTIONAL
MATERIALS**

www.afm-journal.de

Figure 2. a) Normalized PL spectrum (black solid line) of Gua_3SbCl_6 powders at room temperature with the corresponding PL excitation spectrum (dashed line). The absorption spectrum (solid grey line) is presented as the Kubelka–Munk transform of the Gua_3SbCl_6 powders reflectivity. The PL excitation and the pseudo-absorption profiles measured at high energies with synchrotron light are reported as red dashed and solid lines, respectively. b) PL decay trace acquired at the PL maximum under pulsed 3.5 eV excitation. The red line is the fit with a single exponential decay function. c) RL spectra of Gua_3SbCl_6 (rescaled by factor of 2.5) and BGO (black line) powders. d) RL decay traces of the same sample before (orange line) and after (grey line) irradiation with ^{60}Co γ-rays (1 MGy). (e) Light yield spectrum of Gua_3SbCl_6 powders obtained exciting the sample with a ^{57}Co γ-ray source. The red line is the result of the fitting of the photoelectric peak with a Gaussian function. Inset: comparison of the LY values obtained from the relative and absolute measurements from "c" and "e". f) RL spectra of non-irradiated (orange line) and irradiated (grey shaded area) Gua_3SbCl_6 powders with 1 MGy of ^{60}Co γ-rays.

parameters are listed on Table S1 (Supporting Information). The shortest Sb-Cl distance is $\approx2.690(4)$ Å, which is larger than four- and five-coordinated $[Sb_2Cl_8]^{2-}$ and $[SbCl_5]^{2-}$ inorganic units.[28] To further elucidate the crystalline lattice structure, bulk Gua_3SbCl_6 SCs were grown for the first time by slow evaporation of anti-solvents in a precursor solution, yielding colorless single crystals of almost one centimeter in size with preferential exposure of the (101) facets (Figures S2 and S3, Supporting Information). The thermostability of the Gua_3SbCl_6 powders was assessed by thermogravimetric analysis (TGA) that evidenced that the they had a robust stability above 250 °C (Figure S4, Supporting Information).

The optical properties of the Gua_3SbCl_6 crystalline powders were then studied by steady-state and time-resolved optical spectroscopy, also using synchrotron light. A qualitative representation of the absorption profile up to 30 eV excitation is obtained by transforming the diffuse reflectance spectrum according to the Kubelka-Munk function,[29] which shows the characteristic atomic-like transition bands of $[SbCl_6]^{3-}$ octahedra (**Figure 2**a). In particular, the absorption bands at ≈3.3, ≈3.7, and ≈4.1 eV are attributed to the optical transition coupling the $^1S_0$ ground state of Sb with its $^3P_1$, $^3P_2$, and $^1P_1$ excited states, respectively.[30] This is further corroborated by the perfect agreement of the spectral position of the transformed reflectivity peaks with the semi-empirical nephelauxetic series introduced by Shi and co-workers within the dielectric theory for complex crystals,[31] which also suggests that the organic cationic sublattice increases the polarizability volume of the Sb—Cl bonds compared to other fully inorganic zero-dimensional perovskite

systems such as Rb_3SbCl_6,[22h] resulting in a ≈0.6 eV redshift of the lowest Sb transition. The PL profile in Figure 2a was relatively broad (full width at half maximum, FWHM ≈390 meV), centered at ≈1.95 eV, in agreement with the radiative recombination of STEs in $[SbCl_6]^{3-}$ octahedra previously observed in other Sb-based systems, where the large PL Stokes shift originates from the transient stretching of Sb—Cl bonds following a Jhan-Teller lattice rearrangement in the excited state.[22h,32]

The measured PL quantum yield was as high as $\Phi_{PL} = 85 \pm 8\%$. The corresponding PL excitation spectrum followed the absorption profile indicating that recombination always occurred from STEs states independently of the excitation energy, up to 40 eV (see also Figure S5, Supporting Information). In Figure 2b, the PL dynamics under pulsed 3.5 eV excitation followed a single exponential kinetics with lifetime of ≈2.5 μs, consistent with the partially allowed nature of the $^3P_1-^1S_0$ transition of Sb. Such results suggest that the electronic isolation of $[SbCl_6]^{3-}$ octahedra effectively prevents the migration of excitation between neighbouring Sb centers, rendering Gua_3SbCl_6 crystals almost unaffected by non-radiative defects and trap sites, as will be discussed later. This picture is further corroborated by the PL spectra acquired at progressively longer delay times (Figure S6, Supporting Information), which were characterized by essentially identical profiles, providing a clear spectroscopic signature of the absence of excitation migration.

Crucially, by exciting the system with soft X-rays, we observed a RL spectrum in close match with the corresponding PL, indicating that, regardless of the excitation energy and the relax-

ADVANCED
SCIENCE NEWS
www.advancedsciencenews.com

ADVANCED
FUNCTIONAL
MATERIALS
www.afm-journal.de

ation path of the photogenerated carriers, radiative recombination always occurred via STEs localized on single $[SbCl_6]^{3-}$ octahedra. Consistently, the RL decay kinetics shown in Figure 2d resembled well the PL dynamics except for a weak additional fast contribution likely due to ionization of the material or to minor nonradiative losses under ionizing excitation. These results are of technological interest for the realizationn of large-area scintillators, ideally unaffected by self-absorption optical losses, and motivate a detailed study of the scintillation performance of this material system. In this light, we quantified the scintillation efficiency of our Gua_3SbCl_6 crystals by performing two independent scintillation experiments aimed at estimating a LY value. First, we compared the RL spectra of the Gua_3SbCl_6 powders with those of a reference $Bi_4Ge_3O_{12}$ (BGO) crystalline powder (LY ≈ 10^4 ph MeV^{-1})[33] obtained under the same experimental conditions (Figure 2c). This approach yielded a LY value as high as 2300 ± 500 ph MeV^{-1}. Such result was further confirmed by the direct measurement of the LY obtained by the experimental observation of the peak associated with the full-energy absorption events occurring in the Gua_3SbCl_6 powders upon excitation with a ^{57}Co γ-source. This isotope decays by electron capture to the 136.5 keV level of ^{57}Fe: this level decays by emission of a 122 keV gamma ray 85.6% of the time and by emission of a 136.5 keV γ-ray 10.7% of the time. The observed peak in Figure 2e is thus due to events where the energy of the γ-rays is fully transferred inside the scintillator by the photoelectric effect or by multiple Compton events: the width of this peak is affected by the overlap of the 122 and 136.5 keV γ-ray lines. Importantly, the photoelectric peak was well reproduced by a Gaussian function centered at 1800 ± 500 ph MeV^{-1}, providing a LY value in good agreement with that obtained by comparison with the reference BGO powder. Such scintillation properties make Gua_3SbCl_6 crystals promising candidates as active materials in high-energy detectors. This potential was further confirmed by their excellent stability to prolonged exposure to ionising radiation. Specifically, to test their hardness to prolonged exposure to γ-rays, we measured the RL intensity before and after irradiation with a cumulative dose as high as 1 MGy delivered by a ^{60}Co source (Figure 2f) conducted at the Calliope irradiation facility (see also the Experimental Section and Figure S7, Supporting Information). Remarkably, despite the large content of organic moieties in their structure, the Gua_3SbCl_6 powders retained over 70% of their initial RL intensity and both the spectral linewidth (FWHM ≈0.56 eV) and RL kinetics remained essentially unchanged compared to the pristine sample, suggesting that the slight RL weakening is probably due to radiation damage suffered by a sub-fraction of the sample.

Next, we investigated in deeper detail the nonradiative processes competing with the emission from our Gua_3SbCl_6 crystals, by performing PL and RL experiments as a function of temperature, T, from 300 K down to 18 K. As shown in **Figure 3**a,b, upon lowering T, both the PL and RL progressively intensified, blueshifted, and narrowed. The T-dependence of the spectral linewidth, $\Gamma(T)$, of both the PL and RL is quantified in Figure 3c through the equation, $\Gamma(T) = 2.36 \times \sqrt{S} \times E_{ph}\sqrt{\coth(\frac{E_{ph}}{k_BT})}$, which is typically used to describe the phonon-related homogeneous broadening of the emission peak (k_B is the Boltzmann constant and S = 5 is the Huang−Rhys factor). Through this
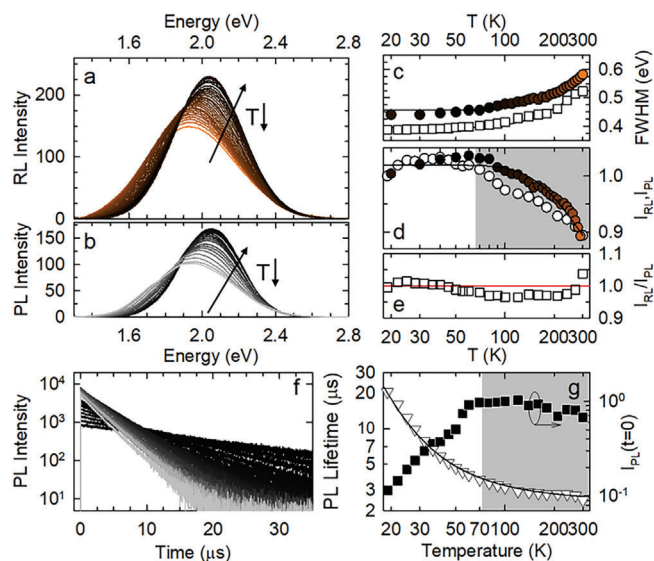

Figure 3. a) RL and b) PL spectra of Gua_3SbCl_6 powders as a function of temperature, T, from 300 to 17 K (from orange(gray) to black curves). c) Spectral linewidth and d) integrated intensity versus T extracted from "a" and "b" (colored symbols correspond to the RL; white symbols correspond to the PL). The black lines are the fitting curves. e) Intensity ratio between the RL and PL signals as a function of T (normalized to the value at 20 K). The red line highlights when $I_{RL}/I_{PL} = 1$, indicating an identical T-dependence for both the PL and RL. f) PL decay curves of Gua_3SbCl_6 powders at decreasing temperature (300 K, black; 18 K grey line). Excitation energy 3.5 eV. g) Zero-delay PL intensity (squares) and PL lifetime (triangles) extracted from "f". The grey shading in panel "d" and "g" highlights the T-regime in which emission occurs primarily from the $^3P_1$ state of $[SbCl_6]^{3-}$ octahedra.

analysis, we obtained a phonon energy, $E_{ph} \approx 32$ meV (≈260 cm^{-1}), which is consistent with the internal vibrational mode of $[SbCl_6]^{3-}$ octahedra.[34] In agreement with the high room temperature PL efficiency, the integrated PL and RL intensity (Figure 3d) increased by only ≈15% upon cooling, with an activation barrier for T-dependent nonradiative losses extracted through Arrhenius fitting of the RL intensity of $E_a = 40$ meV, which is consistent with the phonon energy found by the analysis of the spectral linewidth. Interestingly, the RL and PL intensity trends with T appeared to be remarkably similar, as highlighted by their $I_{RL}(T)/I_{PL}(T)$ ratio reported in Figure 3e thus indicating that the luminescence and scintillation processes are affected by similar, nearly negligible multi-phonon losses. Consistent with the suppression of nonradiative thermal losses between 300 and 100 K, the PL decay traces highlighted ≈15% lengthening of the PL lifetime from 2.7 to 3.1 μs in the same T-range (Figure 3f). For lower temperatures, the PL lifetime underwent drastic deceleration reaching 20 μs at T = 18 K, accompanied by a steep decrease of the initial PL intensity (Figure 3g). This effect is known to be the result of the fine structure of the Sb-related STEs featuring a higher energy, partially bright $^3P_1$ state (the $^3P_1 \rightarrow ^1S_0$ transition is parity forbidden) separated by a lower lying dark state $^3P_0$ state weakly coupled to the ground state by a forbidden transition with negligible oscillator strength.[22h] We were able to fit the experimental PL decay curves in the whole 300–18 K range with a single exponential decay function, resulting in the T-dependent PL life-
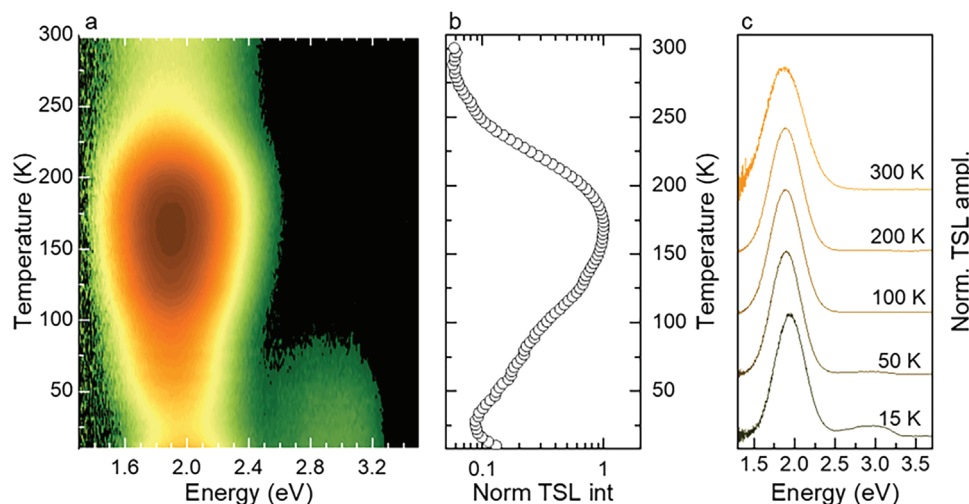
**ADVANCED
SCIENCE NEWS**

www.advancedsciencenews.com

**ADVANCED
FUNCTIONAL
MATERIALS**

www.afm-journal.de

Figure 4. a) Contour plot of the spectrally-resolved TSL intensity as a function of T in the 10–300 K range, obtained after a 5 Gy X-ray dose at 10 K. b) T-dependence of the integrated TSL intensity as extracted from panel "a" and c) TSL spectra at T = 15, 50, 100, 200, and 300 K, vertically shifted for clarity.

times reported in Figure 3g that were then well reproduced by the equation, $\tau(T) = (1 + \exp(-\Delta/k_B T))/(\tau_n^{-1} + \tau_m^{-1}\exp(-\Delta/k_B T))$ where $\tau_{n,m}$ are the intrinsic PL lifetimes of the energy levels $^3P_0$ and $^3P_1$ respectively, and $\Delta \approx 5.5$ meV is their energy difference, in good agreement with previous results on both bulk and nanocrystalline Sb halides.[20a,22d,24b,30a,35]

Finally, to gather deeper insights onto the nature of the trap states responsible for the residual nonradiative losses in Gua_3SbCl_6 crystals, we performed TSL experiments that directly reveal the thermally induced de-trapping of charges from the trap states, providing direct information about their energy position within the semiconductor energy gap. A typical TSL experiment consists in exposing the sample to a predetermined dose of soft X-rays while maintaining it at cryogenic temperature where the populated trap states are stable. The sample, kept in dark and in unstimulated conditions, was slowly warmed up to room temperature while monitoring the stimulated luminescence resulting from the charges that progressively gain enough thermal energy to jump back to the emissive states from the localized traps. Specifically, we irradiated the Gua_3SbCl_6 crystals with soft X-rays (E_{max} = 20 keV) for 15 minutes (corresponding to an overall dose of 5 Gy) and then increased the temperature from 10 to 300 K with a rate of 0.1 Ks^{-1}. The resulting TSL contour plot is reported in **Figure 4**a, and it is dominated by an intense emission peak appearing in the 150–200 K T-range and centered at 1.9 eV.

In Figure 4b, we report the spectrally-integrated TSL signal as a function of temperature (the so-called glow curve), which highlights the broad TSL signal (FWHM ≈90 K) centered at T = 170 K, suggesting the presence of a significantly large distribution of trap states.[36] To quantitatively determine the energy depth of the trap states responsible for the TSL signal, we performed a partial cleaning analysis and applied the initial rise method (see Supplementary Discussion 1, Supplementary Figure S8 for the calculation details),[37] which leads to an energy depth range spanning from 200 ± 12 to 370 ± 20 meV. It is also worth noting that, at any temperature, the TSL signal arose from the Sb-centers,

as highlighted in Figure 4c, showing essentially no modification in the recorded TSL spectra from T = 15 to 300 K, centered at ≈1.9 eV, and in very good agreement with the PL and RL spectra discussed above, further corroborating that the only emissive centers are the distorted $[SbCl_6]^{3-}$ octahedra. We highlight that the weak signal observed at ≈2.9 eV at low temperatures is probably associated to charges trapped in shallow states (this signal is absent for T > 70 K) that undergo radiative recombination from the organic Gua layers. Such an effect is tentatively ascribed to the suppressed charge migration in the Gua_3SbCl_6 crystals at low temperature, thus making emission from the Gua molecules detectable, despite still drastically less intense than emission from the $[SbCl_6]^{3-}$ octahedra.

3. Conclusion

In conclusion, we reported the optical and scintillation properties of a Sb-based hybrid crystals composed of isolated $[SbCl_6]^{3-}$ octahedra separated by layers of Gua^+ molecules, showing >1.3 eV large intrinsic Stokes shift with UV absorption and highly efficient, orange emission. Spectrally- and time-resolved PL experiments as a function of temperature have demonstrated that the minor nonradiative recombination channels affect the exciton prior the STE formation and are assisted by phonon modes quenched at cryogenic temperatures (T < 50 K). Interestingly, the very similar T-dependence of the PL and RL experiments indicate that the optical response of the Gua_3SbCl_6 crystals shows no appreciable modification by increasing the excitation energy from the UV up to the X-ray energy region (i.e., from 3.5 to 20 keV). Such results, combined with the high Φ_{PL} at room temperature (85%), suggest excellent scintillation properties, as confirmed by the light yield value as high as ≈2000 ph MeV^{-1} using 124 keV gamma ray source. Finally, TSL experiments evidenced that the traps responsible for the remnant charge trapping pathways in Gua_3SbCl_6 crystals are featured by a broad distribution of energy depths.

Supporting Information

Acknowledgements

Conflict of Interest

The authors declare no conflict of interest.

Data Availability Statement

The data that support the findings of this study are available from the corresponding author upon reasonable request.

Keywords

[1] C. Dujardin, E. Auffray, E. Bourret-Courchesne, P. Dorenbos, P. Lecoq, M. Nikl, A. N. Vasil'Ev, A. Yoshikawa, R. Y. Zhu, *IEEE Trans. Nucl. Sci.* **2018**, *65*, 1977.

[2] a) J. Knödlseder, *C. R. Phys.* **2016**, *17*, 663; b) M. L. McConnell, P. F. Bloser, J. Legere, J. M. Ryan, *J. Phys.: Conf. Ser.* **2016**, *763*, 012008.

[3] a) J. H. Baker, N. Z. Galunov, A. M. Stepanenko, O. A. Tarasenko, *Radiat. Meas.* **2004**, *38*, 817; b) J. H. Baker, N. Z. Galunov, O. A. Tarasenko, presented at *2007 IEEE Nuclear Science Sympos. Conf. Record*, IEEE, Honolulu, HI, USA **2007**.

[4] a) D. V. Kalaga, A. V. Kulkarni, R. Acharya, U. Kumar, G. Singh, J. B. Joshi, *J. Taiwan Inst. Chem. Eng.* **2009**, *40*, 602; b) C. Szeles, *Phys. Status Solidi B* **2004**, *241*, 783.

[5] a) L. Kuen, J. W. Martin, I. A. B. Garson, M. Beilicke, Q. Guo, Q. Li, G. D. Geronimo, M. Groza, A. Burger, H. Krawczynski, presented at *Proc. SPIE*, SPIE, Orlando, FL, USA, **2010**; b) G. Zentai, *Int. J. Signal Imag. Syst. Eng.* **2010**, *3*, 13.

[6] C. Kim, W. Lee, A. Melis, A. Elmughrabi, K. Lee, C. Park, J.-Y. Yeom, *Crystals* **2021**, *11*, 669.

[7] C. W. E. v. Eijk, *Phys. Med. Biol.* **2002**, *47*, R85.

[8] A. Owens, *IEEE Trans. Nucl. Sci.* **2008**, *55*, 1430.

[9] P. Lecoq, in *Particle Physics Reference Library Detectors for Particles and Radiation*, (Eds: C. W. Fabjan, H. Schopper), Springer International Publishing, Cham **2020**, pp. 45.

[10] G. F. Knoll, in *Radiation Detection and Measurement*, John Wiley & Sons, Hoboken, NJ, USA **2010**.

[11] P. Lecoq, *Nucl. Instrum. Methods Phys. Res., Sect. A* **2016**, *809*, 130.

[12] a) Y. Zhou, J. Chen, O. M. Bakr, O. F. Mohammed, *ACS Energy Lett.* **2021**, *6*, 739; b) F. Zhou, Z. Li, W. Lan, Q. Wang, L. Ding, Z. Jin, *Small Methods* **2020**, *4*, 2000506.

[13] a) D. S. McGregor, *Annu. Rev. Mater. Res.* **2018**, *48*, 245; b) P. Dorenbos, J. T. M. de Haas, C. W. E. van Eijk, *IEEE Trans. Nucl. Sci.* **1995**, *42*, 2190.

[14] T. J. Hajagos, C. Liu, N. J. Cherepy, Q. Pei, *Adv. Mater.* **2018**, *30*, 1706956.

[15] F. Carulli, F. Cova, L. Gironi, F. Meinardi, A. Vedda, S. Brovelli, *Adv. Opt. Mater.* **2022**, *10*, 2200419.

[16] a) A. Vedda, M. Fasoli, M. Nikl, V. V. Laguta, E. Mihokova, J. Pejchal, A. Yoshikawa, M. Zhuravleva, *Phys. Rev. B* **2009**, *80*, 045113; b) X. Y. Liu, G. Pilania, A. A. Talapatra, C. R. Stanek, B. P. Uberuaga, *ACS Appl. Mater. Interfaces* **2020**, *12*, 46296; c) M. Nikl, V. V. Laguta, A. Vedda, *Phys. Status Solidi B* **2008**, *245*, 1701; d) M. Nikl, A. Yoshikawa, *Adv. Opt. Mater.* **2015**, *3*, 463; e) M. Kitaura, S. Watanabe, K. Kamada, K. Jin Kim, M. Yoshino, S. Kurosawa, T. Yagihashi, A. Ohnishi, K. Hara, *Appl. Phys. Lett.* **2018**, *113*, 041906; f) V. Babin, P. Bohacek, L. Grigorjeva, M. Kučera, M. Nikl, S. Zazubovich, A. Zolotarjovs, *Opt. Mater.* **2017**, *66*, 48.

[17] C. Dujardin, E. Auffray, E. Bourret-Courchesne, P. Dorenbos, P. Lecoq, M. Nikl, A. N. Vasil'ev, A. Yoshikawa, R. Y. Zhu, *IEEE Trans. Nucl. Sci.* **2018**, *65*, 1977.

[18] a) T. Yang, F. Li, R. Zheng, *Mater. Adv.* **2021**, *2*, 6744; b) Q. Hu, C. Zhang, X. Wu, G. Liang, L. Wang, X. Niu, Z. Wang, W. D. Si, Y. Han, R. Huang, J. Xiao, D. Sun, *Angew.s Chem., Int. Ed. Engl.* **2023**, *62*, e202217784.

[19] a) V. Morad, Y. Shynkarenko, S. Yakunin, A. Brumberg, R. D. Schaller, M. V. Kovalenko, *J. Am. Chem. Soc.* **2019**, *141*, 9764; b) J. Cao, Z. Guo, S. Zhu, Y. Fu, H. Zhang, Q. Wang, Z. Gu, *ACS Appl. Mater. Interfaces* **2020**, *12*, 19797; c) W. Naewthong, W. Juntapo, R. Amarit, K. Duangkanya, S. Sumriddetchkajorn, T. Rungseesumran, N. Kamwang, Y. Tariwong, J. Kaewkhao, A. Kopwitthaya, *Opt. Mater. Express* **2021**, *12*, 308; d) M. Li, Z. Cheng, X. Wang, Z. Yu, M. Zhou, H. Miao, W. Zhaxi, W. Huang, X. Ma, Q. Chen, S. Jiang, Q. Zhang, D. Wu, *J. Phys. Chem. Lett.* **2021**, *12*, 8237.

[20] a) B. Zhang, V. Pinchetti, J. Zito, A. Ray, A. E. M. Melcherts, M. Ghini, A. Pianetti, I. Infante, S. Brovelli, L. De Trizio, L. Manna, *ACS Energy Lett.* **2021**, *6*, 3952; b) D. Zhu, M. L. Zaffalon, V. Pinchetti, R. Brescia, F. Moro, M. Fasoli, M. Fanciulli, A. Tang, I. Infante, L. De Trizio, S. Brovelli, L. Manna, *Chem. Mater.* **2020**, *32*, 5897; c) H. Zhao, R. Sun, Z. Wang, K. Fu, X. Hu, Y. Zhang, *Adv. Funct. Mater.* **2019**, *29*, 1902262; d) P. Arunkumar, H. B. Cho, K. H. Gil, S. Unithrattil, Y. H. Kim, W. Bin Im, *Nat. Commun.* **2018**, *9*, 4691; e) Y. Jing, Y. Liu, J. Zhao, Z. Xia, *J. Phys. Chem. Lett.* **2019**, *10*, 7439.

[21] Q. He, C. Zhou, L. Xu, S. Lee, X. Lin, J. Neu, M. Worku, M. Chaaban, B. Ma, *ACS Mater. Lett.* **2020**, *2*, 633.

[22] a) H. Arfin, A. S. Kshirsagar, J. Kaur, B. Mondal, Z. Xia, S. Chakraborty, A. Nag, *Chem. Mater.* **2020**, *32*, 10255; b) B. M. Benin, K. M. McCall, M. Worle, V. Morad, S. Yakunin, Y. Shynkarenko, M. V. Kovalenko, *Angew. Chem., Int. Ed.* **2020**, *59*, 14490; c) E. W. J. L. Oomen, G. J. Dirksen, *Mater. Res. Bull.* **1985**, *20*, 453; d) V. Pinchetti, F. Moro, B. Zhang, M. Fanciulli, L. De Trizio, F. Meinardi, L. Manna, S. Brovelli, *ACS Energy Lett.* **2022**, *7*, 1566; e) P. Han, C. Luo, S. Yang, Y. Yang, W. Deng, K. Han, *Angew. Chem., Int. Ed.* **2020**, *59*, 12709; f) Y. Jing, Y. Liu, X. Jiang, M. S. Molokeev, Z. Lin, Z. Xia, *Chem. Mater.* **2020**, *32*, 5327; g) M. B. Gray, S. Hariyani, T. A. Strom, J. D. Majher, J. Brgoch, P. M. Woodward, *J. Mater. Chem. C* **2020**, *8*, 6797; h) D. Zhu,

**ADVANCED
SCIENCE NEWS**

www.advancedsciencenews.com

**ADVANCED
FUNCTIONAL
MATERIALS**

www.afm-journal.de

M. L. Zaffalon, J. Zito, F. Cova, F. Meinardi, L. De Trizio, I. Infante, S. Brovelli, L. Manna, *ACS Energy Lett.* **2021**, *6*, 2283; i) J. D. Majher, M. B. Gray, T. Liu, N. P. Holzapfel, P. M. Woodward, *Inorg. Chem.* **2020**, *59*, 14478.

[23] a) J. Grafmeyer, J. C. Bourcet, J. Janin, J. P. Denis, J. Loriers, *J. Lumin.* **1976**, *11*, 369; b) E. W. J. L. Oomen, R. C. M. Peeters, W. M. A. Smit, G. Blasse, *J. Solid State Chem.* **1988**, *73*, 151; c) E. W. J. L. Oomen, L. C. G. van Gorkom, W. M. A. Smit, G. Blasse, *J. Solid State Chem.* **1986**, *65*, 156; d) A. Ranfagni, D. Mugnai, M. Bacci, G. Viliani, M. P. Fontana, *Adv. Phys.* **2006**, *32*, 823.

[24] a) E. W. J. L. Oomen, W. M. A. Smit, G. Blasse, *Chem. Phys. Lett.* **1984**, *112*, 547; b) E. W. J. L. Oomen, W. M. A. Smit, G. Blasse, *Phys. Rev. B* **1988**, *37*, 18.

[25] S. Wu, W. Li, J. Hu, P. Gao, *J. Mater. Chem. C* **2020**, *8*, 13603.

[26] M. Xia, Z. Xie, H. Wang, T. Jin, L. Liu, J. Kang, Z. Sang, X. Yan, B. Wu, H. Hu, J. Tang, G. Niu, *Adv. Mater.* **2023**, *35*, 2211769.

[27] a) N. Zaitseva, A. Glenn, A. Mabe, L. Carman, S. Payne, *Int. J. Mod. Phys.: Conf. Ser.* **2020**, *50*, 2060003; b) M. Cieślak, K. Gamage, R. Glover, *Crystals* **2019**, *9*, 480.

[28] C. Sun, Z. Deng, Z. Li, Z. Chen, X. Zhang, J. Chen, H. Lu, P. Canepa, R. Chen, L. Mao, *Angew. Chem., Int. Ed. Engl.* **2023**, *62*, 202216720.

[29] S. Landi, I. R. Segundo, E. Freitas, M. Vasilevskiy, J. Carneiro, C. J. Tavares, *Solid State Commun.* **2022**, *341*, 114573.

[30] a) E. W. J. L. Oomen, W. M. A. Smit, G. Blasse, *J. Phys. C: Solid State Phys.* **1986**, *19*, 3263; b) B. Zhou, Z. Liu, S. Fang, H. Zhong, B. Tian, Y. Wang, H. Li, H. Hu, Y. Shi, *ACS Energy Lett.* **2021**, *6*, 3343.

[31] L. L. Wang, H. B. Li, Y. H. Guo, H. Y. Jiang, Q. Wang, C. Y. Ren, J. S. Shi, *J. Am. Ceram. Soc.* **2015**, *98*, 2146.

[32] X. Zhu, M. Du, J. Feng, H. Wang, Z. Xu, L. Wang, S. Zuo, C. Wang, Z. Wang, C. Zhang, X. Ren, S. Priya, D. Yang, S. F. Liu, *Angew. Chem., Int. Ed. Engl.* **2021**, *60*, 4238.

[33] a) I. Holl, E. Lorenz, G. Mageras, *IEEE Trans. Nucl. Sci.* **1988**, *35*, 105; b) M. Moszynski, M. Kapusta, M. Mayhugh, D. Wolski, S. O. Flyckt, *IEEE Trans. Nucl. Sci.* **1997**, *44*, 1052; c) C. W. E. van Eijk, *Nucl. Instrum. Methods Phys. Res., Sect. A* **2001**, *460*, 1.

[34] a) T. Birchall, R. D. Myers, *Inorg. Chem.* **2002**, *22*, 1751; b) M. Gjikaj, T. Xie, W. Brockner, *Z. Anorg. Allg. Chem.* **2009**, *635*, 1036.

[35] E. W. J. L. Oomen, G. J. Dirksen, W. M. A. Smit, G. Blasse, *J. Phys. C: Solid State Phys.* **1987**, *20*, 1161.

[36] a) F. Cova, F. Moretti, C. Dujardin, N. Chiodini, A. Vedda, *J. Phys. Chem. C* **2021**, *125*, 11489; b) S. Liu, J. A. Mares, X. Feng, A. Vedda, M. Fasoli, Y. Shi, H. Kou, A. Beitlerova, L. Wu, C. D'Ambrosio, Y. Pan, M. Nikl, *Adv. Opt. Mater.* **2016**, *4*, 731.

[37] S. W. S. McKeever, in *Thermoluminescence of Solids*, Cambridge University Press, Cambridge **1985**.